

## Article

# Ce<sup>3+</sup>/Ce<sup>4+</sup>-Doped ZrO<sub>2</sub>/CuO Nanocomposite for Enhanced Photocatalytic Degradation of Methylene Blue under Visible Light

Manh Nhuong Chu <sup>1,\*</sup>, Lan T. H. Nguyen <sup>1</sup>, Mai Xuan Truong <sup>1</sup>, Tra Huong Do <sup>1</sup>, Thi Tu Anh Duong <sup>1</sup>, Loan T. T. Nguyen <sup>1</sup>, Mai An Pham <sup>2</sup>, Thi Kim Ngan Tran <sup>3,\*</sup>, Thi Cam Quyen Ngo <sup>3</sup> and Van Huan Pham <sup>4</sup>

<sup>1</sup> Faculty of Chemistry, Thai Nguyen University of Education, Thai Nguyen City 24000, Vietnam; lanth.chem@tnue.edu.vn (L.T.H.N.); truongmx@tnue.edu.vn (M.X.T.); huongdt.chem@tnue.edu.vn (T.H.D.); anhdt@tnue.edu.vn (T.T.A.D.); loannt@tnue.edu.vn (L.T.T.N.)

<sup>2</sup> Faculty of Physics, Thai Nguyen University of Education, Thai Nguyen City 24000, Vietnam; anpm@tnue.edu.vn

<sup>3</sup> Institute of Applied Technology and Sustainable Development, Nguyen Tat Thanh University, Ho Chi Minh City 700000, Vietnam; ntcquyen@ntt.edu.vn

<sup>4</sup> Advanced Institute of Science and Technology, Hanoi University of Science and Technology, Hanoi City 100000, Vietnam; phamhuannb@gmail.com

\* Correspondence: nhuongcm@tnue.edu.vn (M.N.C.); nganttk@ntt.edu.vn (T.K.N.T.)

**Abstract:** In recent years, photocatalysis has been used as an environmentally friendly method for the degradation of organic pigments in water. In this study, Ce<sup>3+</sup>/Ce<sup>4+</sup>-doped ZrO<sub>2</sub>/CuO as a mixed semiconductor oxide was successfully prepared by a one-step hydrothermal method. The Ce<sup>3+</sup>/Ce<sup>4+</sup>-doped ZrO<sub>2</sub>/CuO has shown high degradation efficiency of methylene blue (MB), and the maximum degradation percentage was observed to be 94.5% at 180 min under irradiation visible light. The photocatalytic activity increases significantly by doping Ce<sup>3+</sup>/Ce<sup>4+</sup> in ZrO<sub>2</sub>/CuO for MB degradation. Ce<sup>3+</sup>/Ce<sup>4+</sup> doping is shown to reduce the (e<sup>-</sup>/h<sup>+</sup>) recombination rate and improve the charge transfer, leading to enhanced photocatalytic activity of materials. The materials were characterized by X-ray diffraction (XRD), scanning electron microscopy (SEM), transmission electron microscopy (TEM), FTIR, EDS, BET and diffuse reflectance spectroscopy (DRS).

**Keywords:** Ce<sup>3+</sup>/Ce<sup>4+</sup>; mixed semiconductor oxide; hydrothermal; photocatalysis; methylene blue



**Citation:** Chu, M.N.; Nguyen, L.T.H.; Truong, M.X.; Do, T.H.; Duong, T.T.A.; Nguyen, L.T.T.; Pham, M.A.; Tran, T.K.N.; Ngo, T.C.Q.; Pham, V.H. Ce<sup>3+</sup>/Ce<sup>4+</sup>-Doped ZrO<sub>2</sub>/CuO Nanocomposite for Enhanced Photocatalytic Degradation of Methylene Blue under Visible Light. *Toxics* **2022**, *10*, 463. <https://doi.org/10.3390/toxics10080463>

Academic Editor: João Fernando Pereira Gomes

Received: 20 June 2022

Accepted: 18 July 2022

Published: 10 August 2022

**Publisher's Note:** MDPI stays neutral with regard to jurisdictional claims in published maps and institutional affiliations.



**Copyright:** © 2022 by the authors. Licensee MDPI, Basel, Switzerland. This article is an open access article distributed under the terms and conditions of the Creative Commons Attribution (CC BY) license (<https://creativecommons.org/licenses/by/4.0/>).

## 1. Introduction

Water pollution is a global environmental problem as it can lead to the decomposition of aquatic ecosystems and can affect human health. Contaminants can include organic or inorganic compounds, metal ions, dyes, phenols, pesticides and detergents. In which the pollution of natural and synthetic organic dyes poses challenges because of their high carcinogenic nature due to the fact they contain azo functional groups that, during decomposition, can form amines and benzidine [1]. Organic dyes are persistent organic pollutants that are resistant to decomposition through chemical and biological processes. The dye molecules are practically non-biodegradable, so they persist longer in the environment, creating potential hazards [2].

Today, water pollution is treated by applying technologies such as adsorption, coagulation, filtration and photocatalysis. In which the heterogeneous photocatalysis method has gained wide scientific attention with high potential for applications [3]. Zirconia (ZrO<sub>2</sub>)-based photocatalysis for wastewater treatment is of great interest because ZrO<sub>2</sub> is a semiconductor oxide with high mechanical strength, is non-toxic, and has high chemical stability and biocompatibility. However, ZrO<sub>2</sub> has a large band gap; the E<sub>g</sub> of ZrO<sub>2</sub> ranges from 3.25 to 5.1 eV, depending on the fabrication method [4]. Therefore, ZrO<sub>2</sub> needs to be irradiated with UV radiation to have a photocatalytic activity. UV radiation constitutes

about 5% of the total electromagnetic radiation output from sunlight, limiting the practical applications of ZrO<sub>2</sub>.

To improve the photocatalytic performance of ZrO<sub>2</sub>, coupling with other semiconductor oxides has been shown to be an effective approach. The coupling produces mixed oxide semiconductors (MOS) that are capable of efficient charge separation due to the transition of electrons and holes generated from one semiconductor to another. CuO is often the semiconductor oxide of choice because it is a p-type semiconductor, has a small band gap of about 1.2 eV, is cheap and is environmentally friendly [5]. Renuka, L., et al., reported the synthesis of ZrO<sub>2</sub>/CuO materials with excellent photocatalytic activity under visible light by a simple combustion method. The photocatalytic activity of ZrO<sub>2</sub>/CuO obtained was 1.5 times higher than that of commercial P25 [6]. Nanda, B., et al., synthesized mesoporous CuO/ZrO<sub>2</sub>-MCM-41 nanocomposites with high photocatalytic activity, the photoreduction of Cr(VI) to Cr(III) had a 99% degradation efficiency in 30 min [7]. The synergistic effect between ZrO<sub>2</sub>, CuO and TiO<sub>2</sub> oxides was also studied by Guerrero-Araque and Diana, et al. Co-catalysts are widely used to promote photocatalytic hydrogen production, especially CuO, which has shown a significant improvement in reaction rates [8].

Another use of low-photocatalytic activity is the electron-hole recombination process that occurs in the semiconductor oxide. In photocatalysis, the photocatalytic activity depends on the ability of the catalyst to create electron-hole pairs. Such an electron-hole pair is called an exciton. The excited electron and hole can recombine and release heat. Such exciton recombination leads to a decrease in photocatalytic activity. To reduce the recombination of electrons and holes, it is common to dope transition metal elements, especially rare earth, to prolongation of the exciton lifetime [9].

Recently, Piña-Pérez and Yanet, et al., doped Ce<sup>3+</sup>/Ce<sup>4+</sup> into Al<sub>2</sub>O<sub>3</sub>, showing significantly improved electron-hole pair separation efficiency. This catalyst was chosen for the photodegradation of other phenolic derivatives such as 4-chlorophenol, p-cresol and 4-nitrophenol. Ce<sup>3+</sup>/Ce<sup>4+</sup>-doped Al<sub>2</sub>O<sub>3</sub> synthesized by the sol-gel method showed better photocatalytic activity (TiO<sub>2</sub>, P25 Degussa) [10]. The redox pair of Ce<sup>4+</sup>/Ce<sup>3+</sup>-doped α-β phase of Bi<sub>2</sub>O<sub>3</sub> was reported by Akshatha, S., et al. The Ce<sup>4+</sup>/Ce<sup>3+</sup>-doped Bi<sub>2</sub>O<sub>3</sub> created a synergistic effect to enhance the photocatalytic activity to degrade Alizarin red S dye [11].

To the best of our knowledge, there are many studies on the doping of Ce<sup>3+</sup>/Ce<sup>4+</sup> ions into oxide semiconductors for photocatalysis. However, the doping of Ce<sup>3+</sup>/Ce<sup>4+</sup> ions into mixed semiconductor oxide is a topic that has not been fully investigated. In this paper, we use the hydrothermal method to prepare Ce<sup>3+</sup>/Ce<sup>4+</sup>-doped ZrO<sub>2</sub>/CuO. The Ce<sup>3+</sup>/Ce<sup>4+</sup>-doped ZrO<sub>2</sub>/CuO mixed oxide semiconductor was used for the photocatalytic degradation of methylene blue (MB). X-ray diffraction (XRD), field emission scanning electron microscopy (FE-SEM), transmission electron microscopy (TEM), infrared spectroscopy (FT-IR), energy dispersive X-ray spectroscopy, spectrophotometry UV-Vis and Brunauer-Emmett-Teller (BET) were studied.

## 2. Materials and Methods

### 2.1. Preparation of the Ce<sup>3+</sup>/Ce<sup>4+</sup>-Doped ZrO<sub>2</sub>/CuO Nanocomposites

The Ce<sup>3+</sup>/Ce<sup>4+</sup>-doped ZrO<sub>2</sub>/CuO nanocomposites were synthesized by the hydrothermal method. All chemicals were purchased from Merck (purity > 99%) and were used without further treatment: ZrCl<sub>4</sub>, Cu(NO<sub>3</sub>)<sub>2</sub>·6H<sub>2</sub>O, Ce(SO<sub>4</sub>)<sub>2</sub>·4H<sub>2</sub>O, NaOH, C<sub>2</sub>H<sub>5</sub>OH, Methylene blue.

In a typical experiment, the molar ratio of ZrO<sub>2</sub>/CuO was taken as 1:1, 10 mmol of ZrCl<sub>4</sub> and 10 mmol of Cu(NO<sub>3</sub>)<sub>2</sub> were dissolved in 50 mL of deionized water, stirred in a magnetic stirrer at room temperature for 30 min. Next, 0–0.8 mmol Ce(SO<sub>4</sub>)<sub>2</sub> was added to the above solution. The mixture is stirred vigorously to obtain a clear and homogeneous mixture. After stirring these mixtures for 30 min, they were added to 10 mL of 2 M NH<sub>3</sub> aqueous solution to gel.

The gel was then transferred into a Teflon-lined 100 mL stainless steel autoclave, which was heated in an oven at 200 °C for 12 h (heated with a Nabertherm furnace, heating rate

5 °C/min). For natural cooling, the entire solution was centrifuged to collect the precipitate and washed with deionized water, and then dried at 80 °C. Pure ZrO<sub>2</sub> and CuO were prepared with the same procedure. Finally, all the prepared powders were calcined at 600 °C for 2 h and then allowed to cool to room temperature for further experiments.

## 2.2. Characterization

The morphology of the Ce<sup>3+</sup>/Ce<sup>4+</sup>-doped ZrO<sub>2</sub>/CuO nanocomposites was evaluated by using a field emission scanning electronic microscope (JEOL, JSM-7600F, JEOL Techniques, Tokyo, Japan). The surface morphology and microstructure of the nanocomposites were characterized by transmission electron microscopy (TEM) made with a (JEOL, JEM 1010, JEOL Techniques, Tokyo, Japan) operating at 200 kV. For the TEM analyses, the powders were dispersed in ethanol by sonication for 5 min.

FT-IR was performed in the range of 4000–400 cm<sup>-1</sup> with the help of (FT-IR using a Perkin–Elmer Spectrum BX spectrometer (PerkinElmer Inc., Wellesley, MA, USA) using KBr pellets to identify the functional groups present in the sample. EDS (Hitachi TM4000Plus Tabletop Microscope (Hitachi High-Tech Corporation, Tokyo, Japan)) was the determining element in the composites. The UV-Vis absorption spectrum was recorded using a (UV-1700 PharmaSpec, Shimadzu, Kyoto, Japan) UV-Visible spectrophotometer. The X-ray powder diffraction patterns were characterized using (XRD, D8 Advance, Bruker, Germany) a diffractometer at room temperature (Cu-Kα radiation) with a nickel filter at a scan rate of 2°/min.

## 2.3. Dye Photodegradation

The photocatalytic activity of Ce<sup>3+</sup>/Ce<sup>4+</sup>-doped ZrO<sub>2</sub>/CuO nanocomposites was evaluated by investigating the degradation of methylene blue (MB). Using 30 mL of the MB solution with a dye concentration of 10 mgL<sup>-1</sup>, which was illuminated under a light-emitting 300W Xenon lamp (sunlight simulation) at irradiance (1 Wcm<sup>-2</sup>). Light filters were used to remove wavelengths λ < 420 nm. The distance from the lamp to the MB solution was 10 cm. To limit the influence of external light, the entire experimental system was placed in a dark chamber. The nanocomposite powder loaded into the MB solution was 20 mg. Then the suspension was stirred for 60 min in the dark to obtain balance adsorption and desorption equilibration of the system. About 3 mL was taken from the suspension at different irradiation times, it was then centrifuged at 4000 rpm for 10 min, and degradation measurements were performed by a UV-Vis spectrophotometer. The photodegradation efficiency was calculated using Equation (1):

$$\%H = \frac{C_0 - C_t}{C_0} \cdot 100 \quad (1)$$

where %H is the photodegradation efficiency, C<sub>0</sub> and C<sub>t</sub> are the concentrations of MB at time 0 and t (min), respectively.

## 3. Results

### 3.1. X-ray Diffraction

The XRD pattern of the Ce<sup>3+</sup>/Ce<sup>4+</sup>-doped ZrO<sub>2</sub>/CuO nanocomposites is shown in Figure 1. All the peaks in the XRD pattern are well indexed and have all crystallized as multiphase at Ce<sup>3+</sup>/Ce<sup>4+</sup> different doping concentrations. ZrO<sub>2</sub>/CuO and Ce<sup>3+</sup>/Ce<sup>4+</sup>-doped ZrO<sub>2</sub>/CuO exists in three phases, namely tetragonal ZrO<sub>2</sub>, monoclinic CuO and orthorhombic CuZrO<sub>3</sub>.

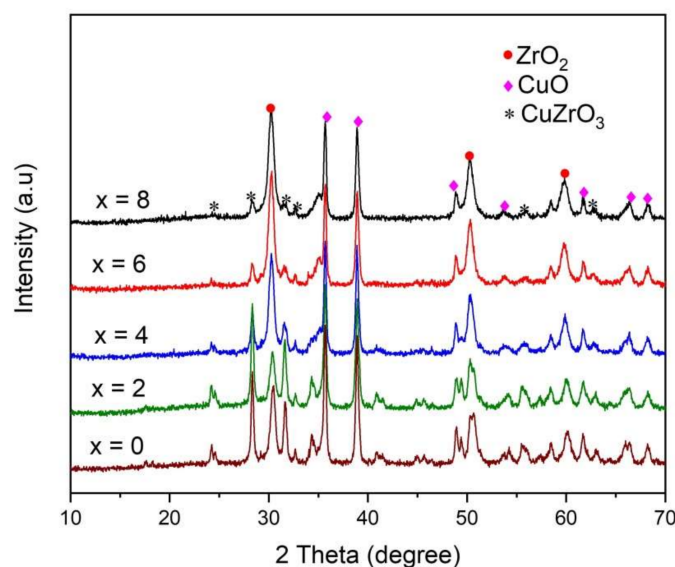


**Figure 1.** XRD patterns of the ZrO<sub>2</sub>/CuO nanocomposite powder with doping of Ce<sup>3+</sup>/Ce<sup>4+</sup> (0–8 mol%).

The diffraction peaks originating at  $2\theta = \sim 30.48^\circ$ ,  $34.35^\circ$ ,  $50.30^\circ$ ,  $50.65^\circ$  and  $60.09^\circ$  correspond to (101), (200), (112), (220) and (202) planes of the tetragonal phase of ZrO<sub>2</sub> (JCPDS No. 00–050–1089), respectively. The diffraction peaks observed at  $2\theta = \sim 35.68^\circ$ ,  $38.89^\circ$ ,  $48.93^\circ$ ,  $53.62^\circ$ ,  $61.70^\circ$ ,  $65.97^\circ$  and  $68.20^\circ$  are associated with (002), (111), ( $-202$ ), (020), ( $-113$ ), (022) and (113) planes, signifying the monoclinic phase of CuO (JCPDS No. 48–1548).

We also observed diffraction peaks at  $2\theta = \sim 24.33^\circ$ ,  $28.29^\circ$ ,  $34.34^\circ$ ,  $55.56^\circ$  and  $61.72^\circ$  corresponded to (012), (112), (013), (313) and (402) planes of CuZrO<sub>3</sub> (PDF Card No. 00–043–0953), respectively. CuZrO<sub>3</sub> can be formed in a hydrothermal process, where the reaction between ZrO<sub>2</sub> and CuO occurs according to the chemical equation:



It is interesting that when the Ce<sup>3+</sup>/Ce<sup>4+</sup> doping concentration changes, the ratio between the phases changes. In the absence of Ce<sup>3+</sup>/Ce<sup>4+</sup> doping, the material exists in all three phases, including tetragonal ZrO<sub>2</sub>, monoclinic CuO and orthorhombic CuZrO<sub>3</sub>. However, when increasing the doping concentration of Ce<sup>3+</sup>/Ce<sup>4+</sup>, the diffraction intensity of the CuZrO<sub>3</sub> phase decreased. According to the authors Dean, James, et al., reported that CuZrO<sub>3</sub> has a perovskite structure; this structure is less stable due to its low energy, which has a thermodynamic preference to decompose into CuO and ZrO<sub>2</sub> [12]. We believe that increasing the concentration of Ce<sup>3+</sup>/Ce<sup>4+</sup> doping increases the ability of phase segregation to CuO and ZrO<sub>2</sub> is preferred.

### 3.2. Microstructure and Morphology of ZrO<sub>2</sub>/CuO-Doped Ce<sup>3+</sup>/Ce<sup>4+</sup> Nanocomposites

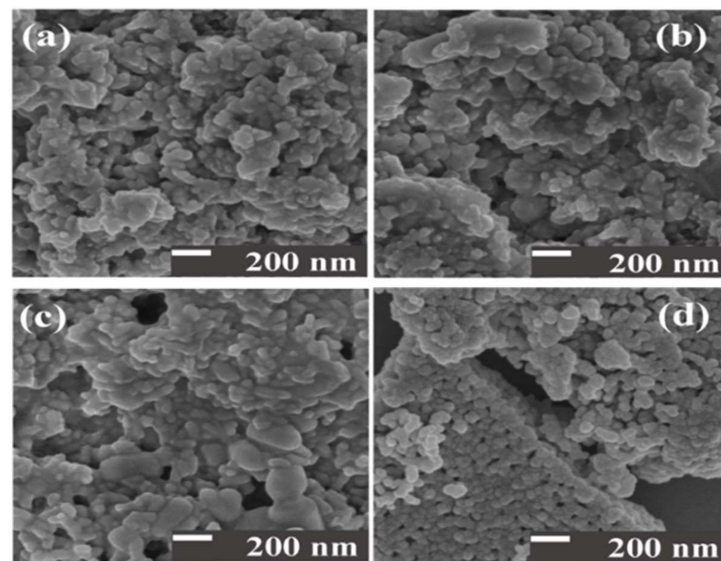
The microstructure of the Ce<sup>3+</sup>/Ce<sup>4+</sup>-doped ZrO<sub>2</sub>/CuO synthesized by the hydrothermal method was analyzed by FE-SEM. Figure 2a–d show that the Ce<sup>3+</sup>/Ce<sup>4+</sup>-doped ZrO<sub>2</sub>/CuO catalysts are spheres with non-uniform size distribution. When the Ce<sup>3+</sup>/Ce<sup>4+</sup> doping concentration changed from 2 mol% to 8 mol%, the morphology of the catalysts was not significantly affected.

The size of the catalyst, as well as the surface area, greatly influence the photocatalytic efficiency. The small size of the material shows that the ability to adsorb the MB on the surface will be better, creating conditions for the oxidizing radicals to easily react with the colourant.

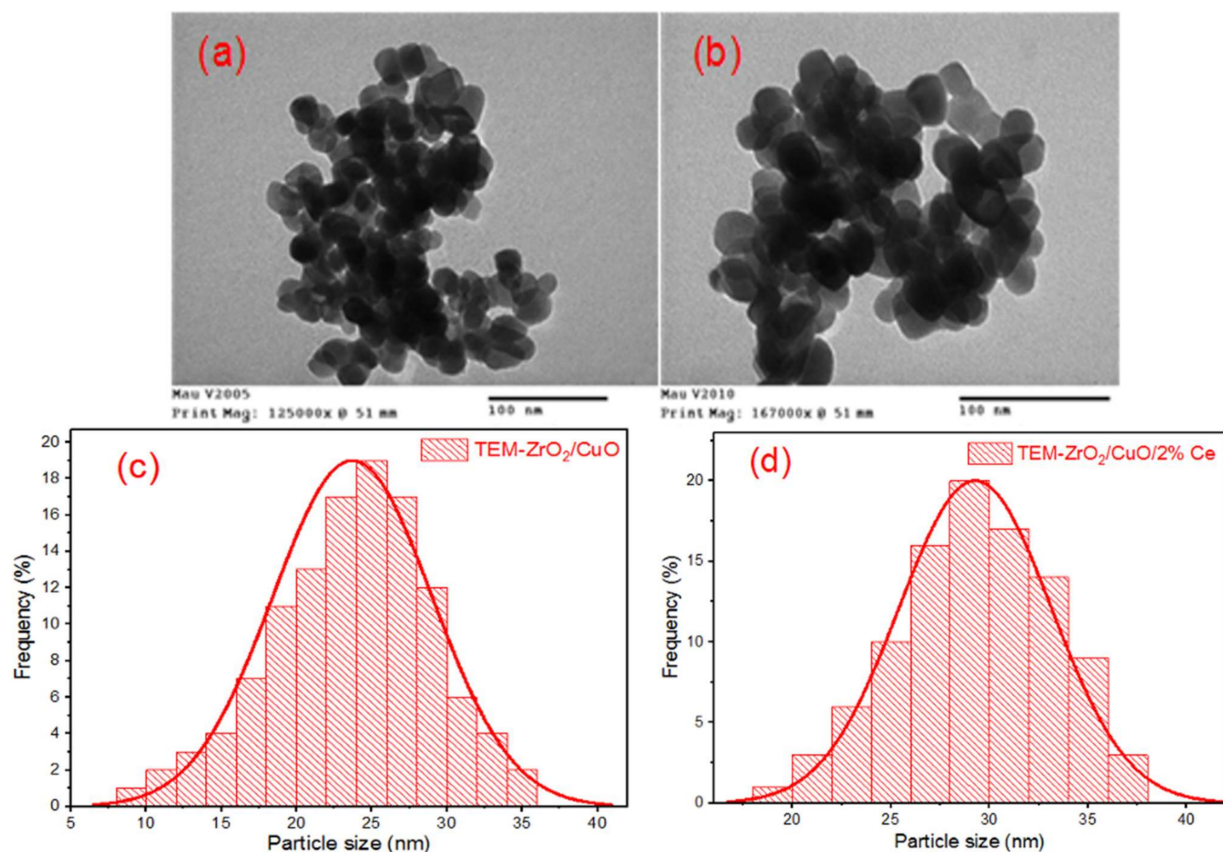
To better understand the shape, size and crystal formation of the Ce<sup>3+</sup>/Ce<sup>4+</sup>-doped ZrO<sub>2</sub>/CuO catalyst, we studied the transmission electron microscopy (TEM) images.

Figure 3 shows that the particle size of the Ce<sup>3+</sup>/Ce<sup>4+</sup>-doped ZrO<sub>2</sub>/CuO catalyst is larger than that of ZrO<sub>2</sub>/CuO. According to the particle size distribution curves in

Figure 3c–d,  $\text{ZrO}_2/\text{CuO}$  concentrates around 20 nm, while  $\text{Ce}^{3+}/\text{Ce}^{4+}$ -doped  $\text{ZrO}_2/\text{CuO}$  concentrates around 30 nm.



**Figure 2.** FE-SEM of  $x$  mol%  $\text{Ce}^{3+}/\text{Ce}^{4+}$ -doped  $\text{ZrO}_2/\text{CuO}$ : (a)  $x = 2$ ; (b)  $x = 4$ ; (c)  $x = 6$ ; (d)  $x = 8$ .

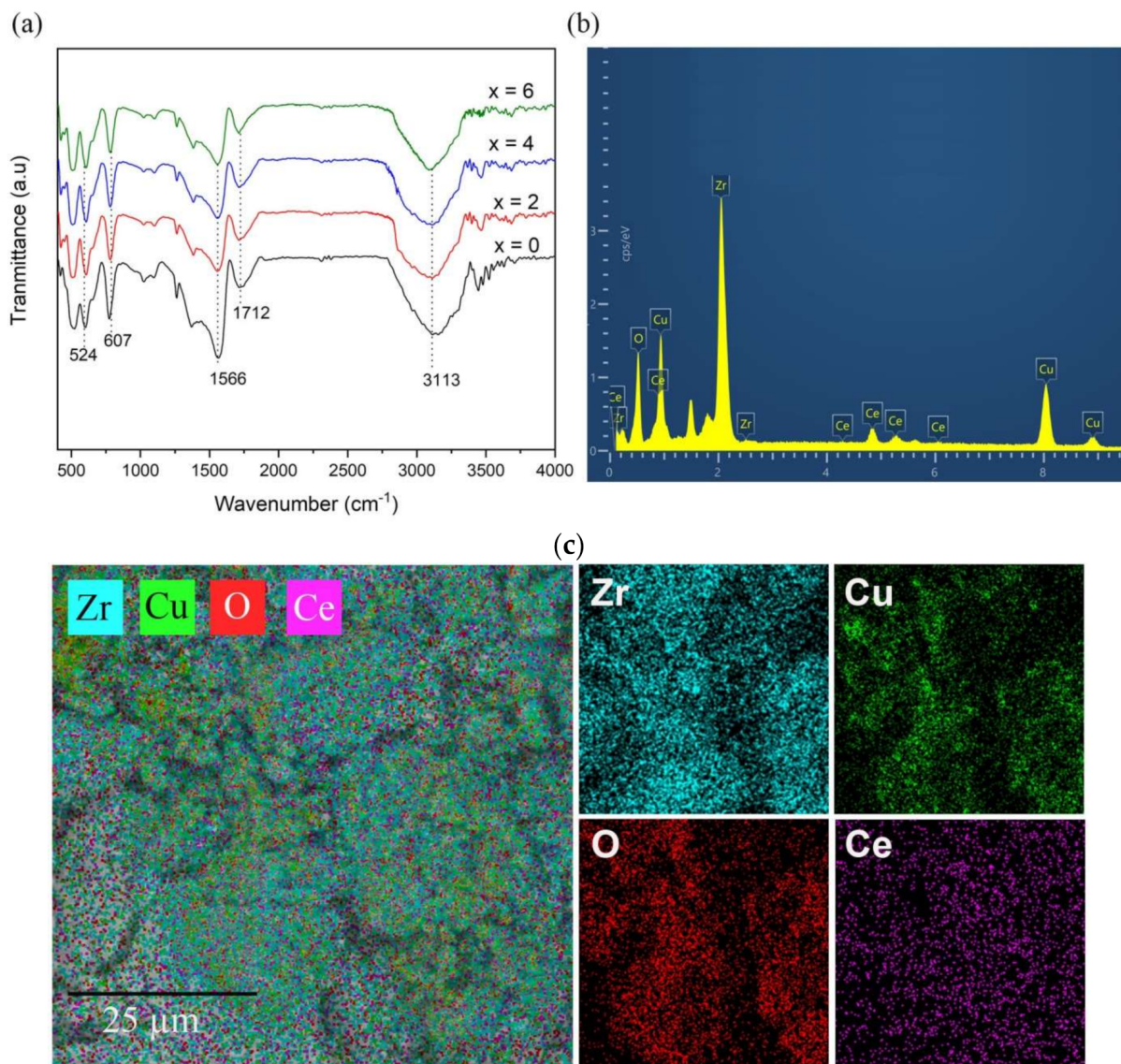


**Figure 3.** TEM and the particle size distribution curve of  $\text{ZrO}_2/\text{CuO}$  (a,c) and 2 mol%  $\text{Ce}^{3+}/\text{Ce}^{4+}$ -doped  $\text{ZrO}_2/\text{CuO}$  (b,d).

### 3.3. Fourier Transform Infrared Spectroscopy and Energy Dispersive X-ray Spectroscopy of the $\text{Ce}^{3+}/\text{Ce}^{4+}$ -Doped $\text{ZrO}_2/\text{CuO}$ Nanocomposites

Figure 4 shows the FT-IR spectra of  $\text{ZrO}_2/\text{CuO}$  and  $\text{Ce}^{3+}/\text{Ce}^{4+}$ -doped  $\text{ZrO}_2/\text{CuO}$ . The  $\text{Ce}^{3+}/\text{Ce}^{4+}$ -doped  $\text{ZrO}_2/\text{CuO}$  materials all have absorption maximums around  $3113\text{--}3153\text{ cm}^{-1}$ ,

which is typical for the –OH group of wet water. The absorption peaks at  $1710\text{--}1712\text{ cm}^{-1}$  and  $1556\text{--}1566\text{ cm}^{-1}$  are characteristic of the vibrations of the Zr–O–H group in the material. In addition, the materials have an absorption maximum of  $601\text{--}607\text{ cm}^{-1}$ , which can be attributed to the vibrational stretching mode of the Cu–O bond. Bands at  $424\text{--}524\text{ cm}^{-1}$  can be assigned to the Zr–O vibration mode in composites.



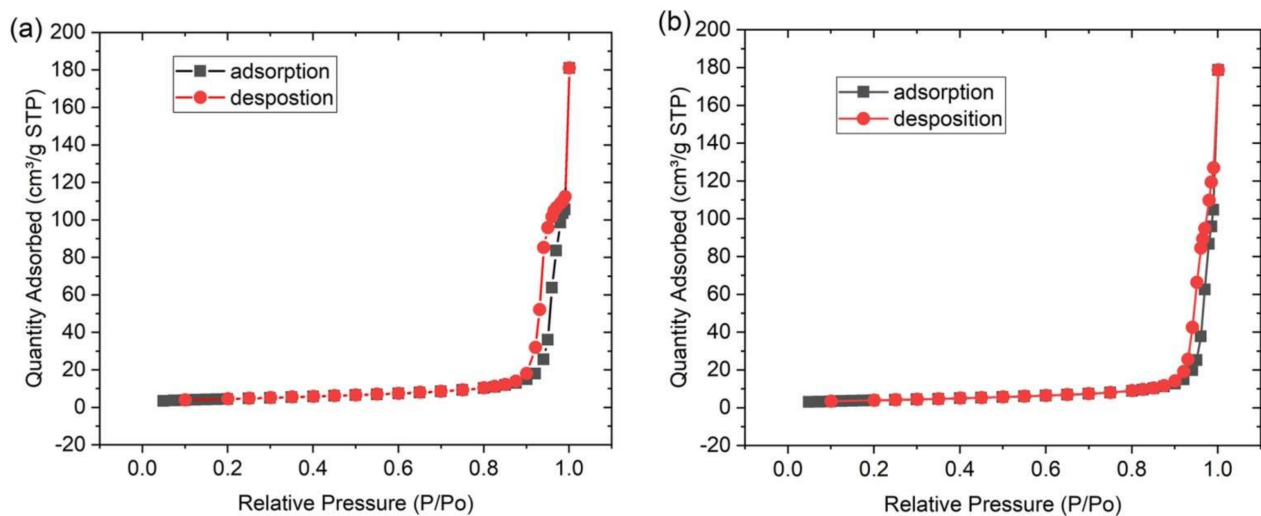
**Figure 4.** (a) FT-IR of  $x$  mol%  $\text{Ce}^{3+}/\text{Ce}^{4+}$ -doped  $\text{ZrO}_2/\text{CuO}$  ( $x = 0; 2; 4; 6$ ), (b) EDS, (c) mapping imaging of 8 mol%  $\text{Ce}^{3+}/\text{Ce}^{4+}$ -doped  $\text{ZrO}_2/\text{CuO}$ .

Figure 4b shows the presence of elements Ce, Zr, Cu and O, confirming the presence of Ce doping in  $\text{ZrO}_2/\text{CuO}$  nanocomposites. We performed EDS mapping, which is equipped with SEM. Figure 4c clearly show the uniform spread of Zr, Cu, O and Ce elements.

### 3.4. Nitrogen Adsorption-Desorption Isotherms of the $\text{Ce}^{3+}/\text{Ce}^{4+}$ -Doped $\text{ZrO}_2/\text{CuO}$ Nanocomposites

The specific surface areas of the  $\text{Ce}^{3+}/\text{Ce}^{4+}$ -doped  $\text{ZrO}_2/\text{CuO}$  and  $\text{ZrO}_2/\text{CuO}$  nanocomposites were determined by measuring the nitrogen adsorption-desorption isotherms, as shown in Figure 5. All of them are all type III adsorption isotherms [13]. The BET surface areas of  $\text{ZrO}_2/\text{CuO}$  and  $\text{Ce}^{3+}/\text{Ce}^{4+}$ -doped  $\text{ZrO}_2/\text{CuO}$  are  $15.59$  and  $13.52\text{ m}^2\text{g}^{-1}$ . The

large surface area of the catalyst facilitates the adsorption of the pigment to the surface of the material, thereby improving the photocatalyst efficiency.



**Figure 5.** Nitrogen adsorption-desorption isotherms of (a)  $\text{ZrO}_2/\text{CuO}$ , and (b) 2 mol%  $\text{Ce}^{3+}/\text{Ce}^{4+}$ -doped  $\text{ZrO}_2/\text{CuO}$ .

### 3.5. UV-Vis Absorption Spectrum of $\text{Ce}^{3+}/\text{Ce}^{4+}$ -Doped $\text{ZrO}_2/\text{CuO}$ Nanocomposites

Figure 6 shows the UV-Vis absorption spectrum and the bandgap energy of the  $\text{Ce}^{3+}/\text{Ce}^{4+}$ -doped  $\text{ZrO}_2/\text{CuO}$ . The results show that the  $\text{Ce}^{3+}/\text{Ce}^{4+}$ -doped  $\text{ZrO}_2/\text{CuO}$  oxide composite material has an absorption region from UV to the visible region (200–1000 nm). To calculate the band gap, the Tauc relation is used:

$$\alpha h\nu = A(h\nu - E_g)^n \quad (3)$$

where  $\alpha$  is the absorption coefficient,  $h$  is the Planck constant,  $\nu$  is the frequency of the incident photon,  $A$  is a constant that depends on the transition probability,  $E_g$  is the band gap energy and  $n$  is an index that depends on the transition probability of the nature of the electronic transition.

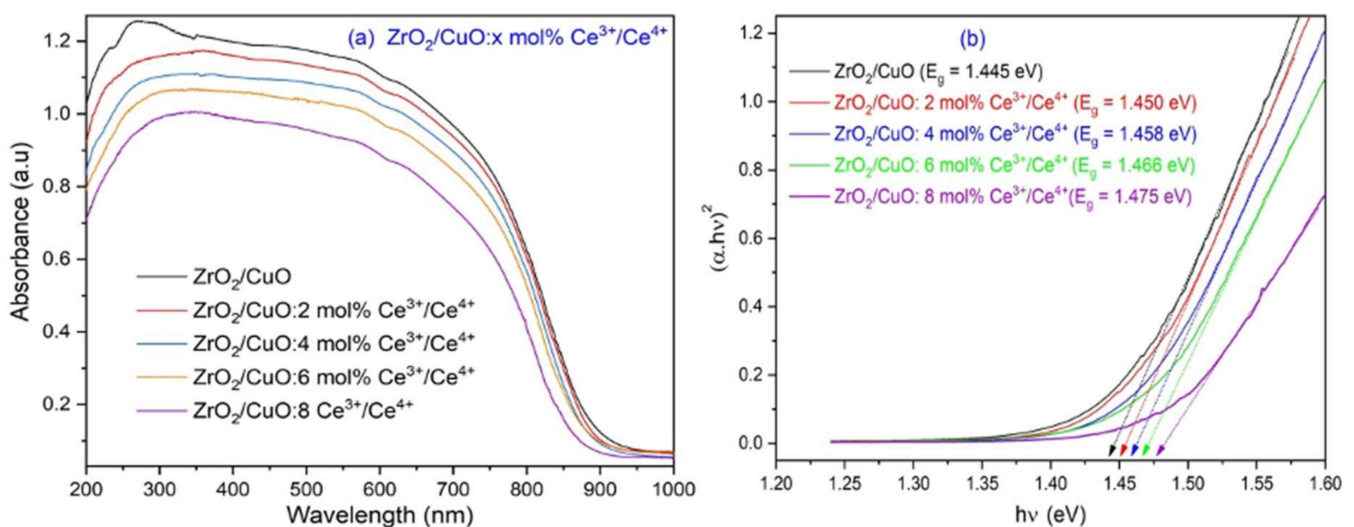


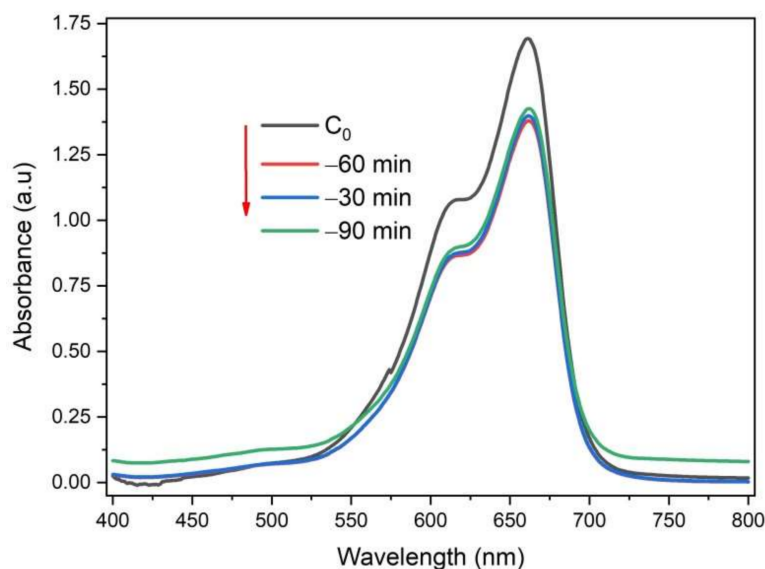
**Figure 6.** (a) The UV-Vis DRS and (b) The Kubelka-Munk energy curve versus the band gap (eV) of the  $x$  mol%  $\text{Ce}^{3+}/\text{Ce}^{4+}$ -doped  $\text{ZrO}_2/\text{CuO}$  ( $x = 0; 2; 4; 6; 8$ ).

The bandgap energy of  $\text{Ce}^{3+}/\text{Ce}^{4+}$ -doped  $\text{ZrO}_2/\text{CuO}$  was found to be in the range of 1.445–1.475 eV. When increasing the  $\text{Ce}^{3+}/\text{Ce}^{4+}$  doping concentration from 0 to 8 mol%, the band gap increased slightly from 1.445 to 1.475 eV. When Ce was doped into  $\text{ZrO}_2/\text{CuO}$ , the 5d and 6s orbitals of Ce overlapping with the d orbitals of Cu and Zr can increase the size of the valence band and also lower the position of its maximum, thereby increasing the band gap of mixed semiconductor oxide. The increase in the optical band gap upon Ce doping is similar to the increase in the band gap of  $\text{Ag}_2\text{O}$  upon Zn doping, as reported by De, Arup Kumar et al. [14]. The decrease in the band gap of the  $\text{ZrO}_2/\text{CuO}$  nanocomposites material compared with that of pure  $\text{ZrO}_2$  is mainly due to the introduction of CuO into the  $\text{ZrO}_2$  host matrix. It was found that when two metals combine, the band gap decreases and thus a shift to the visible region is observed [15].

The narrowing of the band gap can be attributed to the appearance of an impurity region (CuO) formed by overlapping impurity states and local states formed by the combination of Cu 2p and Zr 3p [7]. This result is similar to previous studies [16]. The photocatalytic reaction is initiated by the absorption of light with an energy equal to or greater than the band gap of the semiconductor. The band gap is in the range of 1.445–1.475 eV, so it is expected that the catalyst material can absorb visible light.

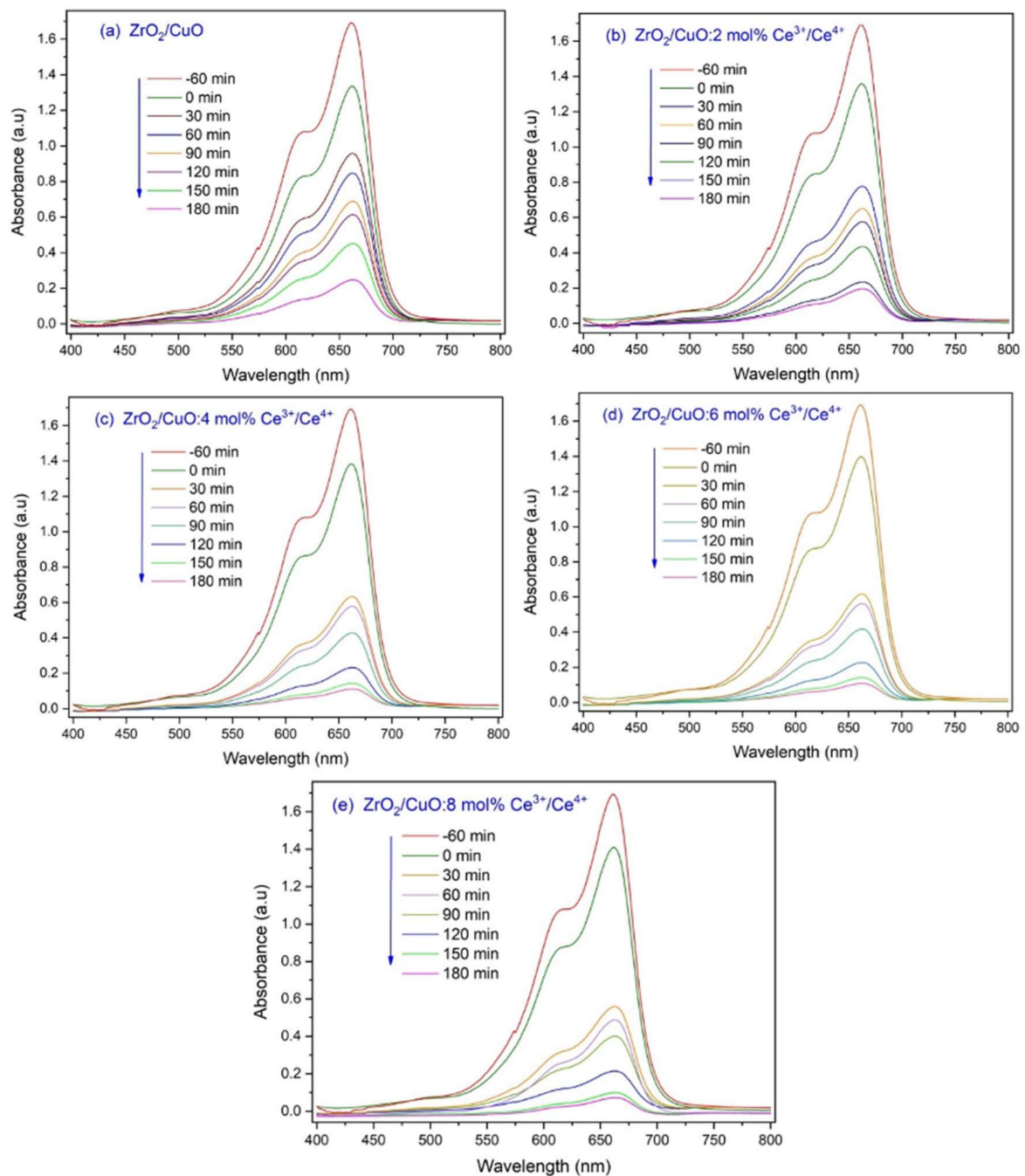
### 3.6. Photocatalytic Activity of $\text{Ce}^{3+}/\text{Ce}^{4+}$ -Doped $\text{ZrO}_2/\text{CuO}$ Nanocomposites

To investigate the adsorption balance, 20 mg of 8 mol%  $\text{Ce}^{3+}/\text{Ce}^{4+}$ -doped  $\text{ZrO}_2/\text{CuO}$  was added into 30 mL of  $10 \text{ mgL}^{-1}$  MB solution. The suspension was stirred in the dark; samples were measured via UV-Vis spectroscopy. Figure 7 shows that after the first 30 min, the concentration of MB strongly decreased, then at 60 min slightly decreased, and at 90 min, the concentration of MB increased slightly (desorption). It is shown that after 60 min of adsorption, equilibration has occurred.



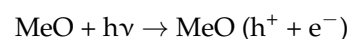
**Figure 7.** UV-Vis spectrum of MB after being adsorbed by  $\text{ZrO}_2/\text{CuO}$ -doped 8 mol%  $\text{Ce}^{3+}/\text{Ce}^{4+}$ .

Figure 8 shows the UV-Vis absorption spectrum of MB under visible light at different times in the presence of  $\text{Ce}^{3+}/\text{Ce}^{4+}$ -doped  $\text{ZrO}_2/\text{CuO}$ . The evolution of MB photodegradation was monitored by measuring the absorbance at the wavelength of about  $\lambda = 662 \text{ nm}$  at different times. The maximum absorption peaks of MB gradually decreased and almost disappeared in 180 min of illumination.

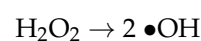
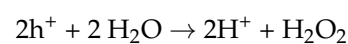
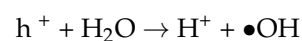


**Figure 8.** UV-Vis absorbance of MB under visible light at different times in the presence of  $x$  mol%  $\text{Ce}^{3+}/\text{Ce}^{4+}$ -doped  $\text{ZrO}_2/\text{CuO}$ : (a)  $x = 0$ ; (b)  $x = 2$ ; (c)  $x = 4$ ; (d)  $x = 6$ ; (e)  $x = 8$ .

The reactions that occur during photocatalysis are described below. The reaction begins by generating excitons on the metal oxide surface (MeO) [17]:



Oxidation reactions due to the photocatalytic effect:



Reduction reaction due to the photocatalytic effect:

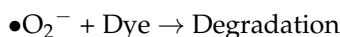
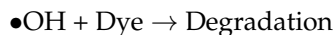
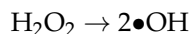
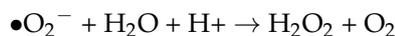
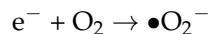
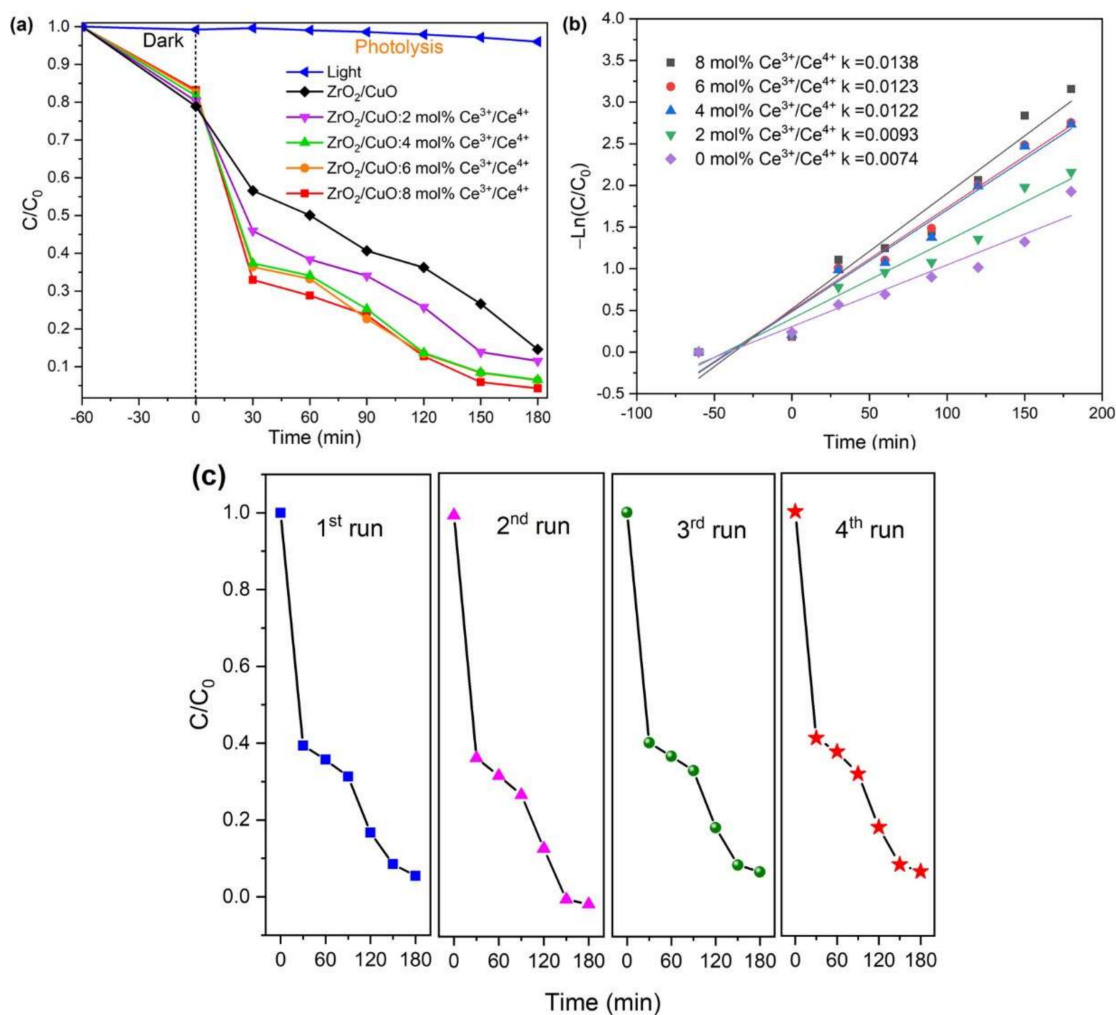


Figure 9a shows the ZrO<sub>2</sub>/CuO catalyst, the photocatalytic efficiency of MB decomposition by Ce<sup>3+</sup>/Ce<sup>4+</sup>-doped ZrO<sub>2</sub>/CuO increased significantly. The Ce<sup>3+</sup>/Ce<sup>4+</sup> doping concentration increased, and the photocatalytic efficiency under visible light also increased. Although the E<sub>g</sub> values of ZrO<sub>2</sub>/CuO and ZrO<sub>2</sub>/CuO-doped Ce<sup>3+</sup>/Ce<sup>4+</sup> were not significantly different, the results showed that the photocatalytic degradation efficiency was enhanced by Ce<sup>3+</sup>/Ce<sup>4+</sup> doping. This could be due to the fact that as the Ce<sup>3+</sup>/Ce<sup>4+</sup> ion concentration increases, an increase in oxygen vacancy defects in the crystal lattice occurs. This leads to the redox pair Ce<sup>3+</sup>/Ce<sup>4+</sup> being capable of shifting between Ce<sub>2</sub>O<sub>3</sub> and CeO<sub>2</sub>, which reduces electron-hole recombination [18].



**Figure 9.** (a) Photodegradation of MB, (b) the reaction rate constant *k* of the MB degradation in the presence of *x* mol% Ce<sup>3+</sup>/Ce<sup>4+</sup> doped ZrO<sub>2</sub>/CuO (*x* = 0; 2; 4; 6; 8), (c) reuse of 8 mol% of Ce<sup>3+</sup>/Ce<sup>4+</sup> doping ZrO<sub>2</sub>/CuO.

The MB degradation processes all show first-order kinetics by plotting  $\ln(C/C_0)$  versus irradiation time,  $t$ . The apparent response rate constant ( $k_{app}$ ) was calculated from the slope of the curve, as illustrated in Figure 9b.

The  $k_{app}$  value continuously increased as the  $Ce^{3+}/Ce^{4+}$  doping concentration increased, with  $x = 0$ ,  $k_{app} = 0.0074 \text{ min}^{-1}$ ;  $x = 2$ ,  $k_{app} = 0.0093 \text{ min}^{-1}$ ;  $x = 4$ ,  $k_{app} = 0.0122 \text{ min}^{-1}$ ;  $x = 6$ ,  $k_{app} = 0.0123 \text{ min}^{-1}$ ; and  $x = 8$ ,  $k_{app} = 0.0138 \text{ min}^{-1}$ . It was shown that 8 mol%  $Ce^{3+}/Ce^{4+}$ -doped  $ZrO_2/CuO$  exhibited the highest  $k_{app} = 0.0138 \text{ min}^{-1}$ , much higher than that of undoped  $ZrO_2/CuO$  with  $Ce^{3+}/Ce^{4+}$ .

Figure 9c shows the stability of the  $Ce^{3+}/Ce^{4+}$ -doped  $ZrO_2/CuO$  nanocomposites. The stability of the MOS material was evaluated by performing photocatalyst recycling experiments for a duration of 180 min. The activity was found to be roughly the same in the two repeated runs, and then there was a slight decrease in the third and fourth runs.

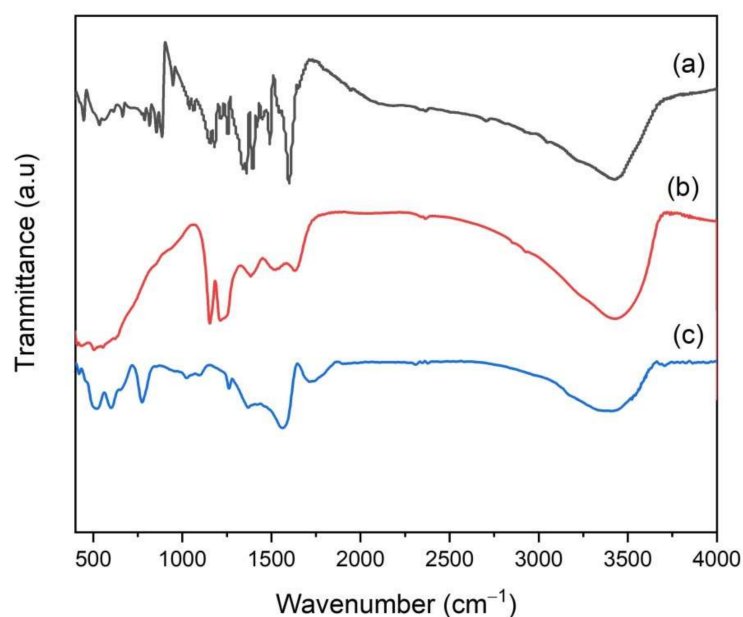
We assume that there is metal-to-metal charge transfer (MMCT). The MMCT effect is assumed to be:  $Zr^{4+}-O-Ce^{4+}$  to  $Zr^{4+}-O-Ce^{3+}$  and  $Zr^{4+}-O-Cu^{2+}$  to  $Zr^{4+}-O-Cu^+$ . The effect is when two different metals in the mixture form an oxygen bridge, which helps electrons and holes move efficiently and avoid recombination, increasing the photocatalytic efficiency of the  $Ce^{3+}/Ce^{4+}$ -doped  $ZrO_2/CuO$  catalyst [19]. Furthermore,  $Ce^{3+}/Ce^{4+}$  ions act as electron-trapping sites reducing charge-pair recombination and thus enhancing photocatalytic activity [20,21].

Table 1 shows the photocatalytic degradation of MB using the various heterojunction photocatalyst. It shows that the combination of semiconductor oxides, or metal ion doping, shows an improved rate constant compared to single semiconductor oxides.

**Table 1.** Photocatalytic degradation of MB dye using the various heterojunction photocatalyst.

Photocatalyst	Synthesis Method	Light Source	Rate Constant ( $\text{min}^{-1}$ )	Reference
$Fe_2O_3$ /graphene/ $CuO$	Solvothermal	Visible	$72.5 \times 10^{-3}$	[22]
$CuO/ZnO$	Impregnation	UV lamp	$182 \times 10^{-3}$	[23]
$ZrO_2/AgCl:Eu^{3+}$	Sol-gel	Visible	$14 \times 10^{-3}$	[24]
C-doped $ZrO_2$	Sol-gel	UVC lamp	$7.3 \times 10^{-3}$	[25]
N- $TiO_2/ZrO_2$	Hydrothermal	UV light	$29 \times 10^{-3}$	[26]
$ZrO_2/CuO$	Combustion	Visible	$11.19 \times 10^{-3}$	[6]
GO- $ZrO_2$	Co-precipitation	Visible	$57.5 \times 10^{-3}$	[27]
$CeO_2$	Precipitation	UV light	$12.1 \times 10^{-3}$	[28]
$V_2O_5-CeO_2$	Precipitation	Visible	$108 \times 10^{-3}$	[29]
$CeO_2/TiO_2$	Precipitation	Visible	$34 \times 10^{-3}$	[30]
$Ce^{3+}/Ce^{4+}$ -doped $ZrO_2/CuO$	Hydrothermal	Visible	$13.8 \times 10^{-3}$	This work

The  $ZrO_2/CuO$ -doped  $Ce^{3+}/Ce^{4+}$  photocatalyst can be reproducible and without destruction. This reproducible process can be confirmed by FT-IR, as shown in Figure 10. It is clear that the characteristic bands of MB, which are at 1383, 1324, 1245, 884 and 670  $\text{cm}^{-1}$ , appear after adsorbing [31], while they disappear after 180 min of irradiation. Combined with the results of photocatalytic reuse experiments, it is proven that the  $Ce^{3+}/Ce^{4+}$ -doped  $ZrO_2/CuO$  nanocomposites have stability.



**Figure 10.** FT-IR spectrum of (a) MB, (b) MB adsorbed onto  $\text{Ce}^{3+}/\text{Ce}^{4+}$ -doped  $\text{ZrO}_2/\text{CuO}$  before irradiation, (c) MB adsorbed on  $\text{Ce}^{3+}/\text{Ce}^{4+}$ -doped  $\text{ZrO}_2/\text{CuO}$  180 min after irradiation.

#### 4. Conclusions

$\text{Ce}^{3+}/\text{Ce}^{4+}$ -doped  $\text{ZrO}_2/\text{CuO}$  nanocomposites have been synthesized by the simple hydrothermal method. The obtained material is a mixed semiconductor oxide  $\text{ZrO}_2$  and  $\text{CuO}$ . The coupling between  $\text{CuO}$  and  $\text{ZrO}_2$  oxides has shown that the light absorption capacity is extended from UV to the visible region. Photocatalytic activity is enhanced when doping  $\text{Ce}^{3+}/\text{Ce}^{4+}$  ions because  $\text{Ce}^{3+}/\text{Ce}^{4+}$  ions have higher separation efficiency of charge carriers, which reduces electron-hole recombination. The  $\text{Ce}^{3+}/\text{Ce}^{4+}$ -doped  $\text{ZrO}_2/\text{CuO}$  nanocomposites showed significantly improved photocatalytic activity. High photocatalysis activity with 94.5% degradation efficiency of MB was achieved after 180 min under visible light irradiation. It is believed that these materials will have promising applications in the wastewater treatment field.

**Author Contributions:** Writing—original draft preparation, M.N.C., L.T.H.N. and V.H.P.; software, M.X.T. and T.H.D.; data curation, T.T.A.D.; conceptualization, M.A.P., T.C.Q.N. and L.T.T.N.; writing—review and editing M.N.C., T.K.N.T. and V.H.P.; Supervision: M.N.C.; L.T.H.N. and M.X.T. All authors have read and agreed to the published version of the manuscript.

**Funding:** This research received no external funding.

**Institutional Review Board Statement:** Not applicable.

**Informed Consent Statement:** Not applicable.

**Data Availability Statement:** All the data are available within the manuscript.

**Acknowledgments:** The authors thank Thai Nguyen University of Education (TNUE, Vietnam) for providing all the necessary facilities to complete this study.

**Conflicts of Interest:** The authors declare no conflict of interest.

#### References

1. Maheshwari, K.; Agrawal, M.; Gupta, A.B. Dye Pollution in Water and Wastewater. In *Novel Materials for Dye-Containing Wastewater Treatment*; Springer: Berlin/Heidelberg, Germany, 2021; pp. 1–25.
2. Alharbi, O.M.L.; Khattab, R.A.; Ali, I. Health and environmental effects of persistent organic pollutants. *J. Mol. Liq.* **2018**, *263*, 442–453. [[CrossRef](#)]
3. Anwer, H.; Mahmood, A.; Lee, J.; Kim, K.-H.; Park, J.-W.; Yip, A.C.K. Photocatalysts for degradation of dyes in industrial effluents: Opportunities and challenges. *Nano Res.* **2019**, *12*, 955–972. [[CrossRef](#)]

4. Reddy, B.M.; Khan, A. Recent advances on TiO<sub>2</sub>-ZrO<sub>2</sub> mixed oxides as catalysts and catalyst supports. *Catal. Rev.* **2005**, *47*, 257–296. [[CrossRef](#)]
5. Fazl, F.; Gholivand, M.B. High performance electrochemical method for simultaneous determination dopamine, serotonin, and tryptophan by ZrO<sub>2</sub>-CuO co-doped CeO<sub>2</sub> modified carbon paste electrode. *Talanta* **2022**, *239*, 122982. [[CrossRef](#)]
6. Renuka, L.; Anantharaju, K.S.; Vidya, Y.S.; Nagaswarupa, H.P.; Prashantha, S.C.; Sharma, S.C.; Nagabhushana, H.; Darshan, G.P. A simple combustion method for the synthesis of multi-functional ZrO<sub>2</sub>/CuO nanocomposites: Excellent performance as Sunlight photocatalysts and enhanced latent fingerprint detection. *Appl. Catal. B Environ.* **2017**, *210*, 97–115. [[CrossRef](#)]
7. Nanda, B.; Pradhan, A.C.; Parida, K.M. Fabrication of mesoporous CuO/ZrO<sub>2</sub>-MCM-41 nanocomposites for photocatalytic reduction of Cr (VI). *Chem. Eng. J.* **2017**, *316*, 1122–1135. [[CrossRef](#)]
8. Guerrero-Araque, D.; Acevedo-Peña, P.; Ramírez-Ortega, D.; Calderon, H.A.; Gómez, R. Charge transfer processes involved in photocatalytic hydrogen production over CuO/ZrO<sub>2</sub>-TiO<sub>2</sub> materials. *Int. J. Hydrogen Energy* **2017**, *42*, 9744–9753. [[CrossRef](#)]
9. Rajendran, S.; Khan, M.M.; Gracia, F.; Qin, J.; Gupta, V.K.; Arumainathan, S. Ce<sup>3+</sup>-ion-induced visible-light photocatalytic degradation and electrochemical activity of ZnO/CeO<sub>2</sub> nanocomposite. *Sci. Rep.* **2016**, *6*, 1–11. [[CrossRef](#)]
10. Piña-Pérez, Y.; Tzompantzi-Morales, F.; Pérez-Hernández, R.; Arroyo-Murillo, R.; Acevedo-Peña, P.; Gómez-Romero, R. Photocatalytic activity of Al<sub>2</sub>O<sub>3</sub> improved by the addition of Ce<sup>3+</sup>/Ce<sup>4+</sup> synthesized by the sol-gel method. Photodegradation of phenolic compounds using UV light. *Fuel* **2017**, *198*, 11–21. [[CrossRef](#)]
11. Akshatha, S.; Sreenivasa, S.; Parashuram, L.; Kumar, V.U.; Sharma, S.C.; Nagabhushana, H.; Kumar, S.; Maiyalagan, T. Synergistic effect of hybrid Ce<sup>3+</sup>/Ce<sup>4+</sup> doped Bi<sub>2</sub>O<sub>3</sub> nano-sphere photocatalyst for enhanced photocatalytic degradation of alizarin red S dye and its NUV excited photoluminescence studies. *J. Environ. Chem. Eng.* **2019**, *7*, 103053. [[CrossRef](#)]
12. Dean, J.; Yang, Y.; Vesper, G.; Mpourmpakis, G. CuZrO<sub>3</sub>: If it exists it should be a sandwich. *Phys. Chem. Chem. Phys.* **2021**, *23*, 23748–23757. [[CrossRef](#)] [[PubMed](#)]
13. Donohue, M.D.; Aranovich, G.L. Classification of Gibbs adsorption isotherms. *Adv. Colloid Interface Sci.* **1998**, *76*, 137–152. [[CrossRef](#)]
14. De, A.K.; Majumdar, S.; Pal, S.; Kumar, S.; Sinha, I. Zn doping induced band gap widening of Ag<sub>2</sub>O nanoparticles. *J. Alloys Compd.* **2020**, *832*, 154127. [[CrossRef](#)]
15. Pelaez, M.; Nolan, N.T.; Pillai, S.C.; Seery, M.K.; Falaras, P.; Kontos, A.G.; Dunlop, P.S.M.; Hamilton, J.W.J.; Byrne, J.A.; O’Shea, K. A review on the visible light active titanium dioxide photocatalysts for environmental applications. *Appl. Catal. B Environ.* **2012**, *125*, 331–349. [[CrossRef](#)]
16. Sapawe, N. Hybridization of zirconia, zinc and iron supported on HY zeolite as a solar-based catalyst for the rapid decolorization of various dyes. *New J. Chem.* **2015**, *39*, 4526–4533. [[CrossRef](#)]
17. Schneider, J.; Matsuoka, M.; Takeuchi, M.; Zhang, J.; Horiuchi, Y.; Anpo, M.; Bahnemann, D.W. Understanding TiO<sub>2</sub> photocatalysis: Mechanisms and materials. *Chem. Rev.* **2014**, *114*, 9919–9986. [[CrossRef](#)]
18. Wang, X.; Zhai, B.; Yang, M.; Han, W.; Shao, X. ZrO<sub>2</sub>/CeO<sub>2</sub> nanocomposite: Two step synthesis, microstructure, and visible-light photocatalytic activity. *Mater. Lett.* **2013**, *112*, 90–93. [[CrossRef](#)]
19. Raees, A.; Jamal, M.A.; Ahmed, I.; Silanpaa, M.; Saad Algarni, T. Synthesis and characterization of CeO<sub>2</sub>/CuO nanocomposites for photocatalytic degradation of methylene blue in visible light. *Coatings* **2021**, *11*, 305. [[CrossRef](#)]
20. Ansari, S.; Khan, M.; Omaish, M.; Kalathil, S.; Lee, J.; Cho, M. Band gap engineering of CeO<sub>2</sub> Nanostructure by electrochemically active biofilm for visible light applications. *RSC Adv.* **2014**, *4*, 16782–16791. [[CrossRef](#)]
21. Khan, M.M.; Ansari, S.A.; Pradhan, D.; Han, D.H.; Lee, J.; Cho, M.H. Defect-induced band gap narrowed CeO<sub>2</sub> nanostructures for visible light activities. *Ind. Eng. Chem. Res.* **2014**, *53*, 9754–9763. [[CrossRef](#)]
22. Nuengmatcha, P.; Porrawatkul, P.; Chanthai, S.; Sricharoen, P.; Limchoowong, N. Enhanced photocatalytic degradation of methylene blue using Fe<sub>2</sub>O<sub>3</sub>/graphene/CuO nanocomposites under visible light. *J. Environ. Chem. Eng.* **2019**, *7*, 103438. [[CrossRef](#)]
23. Acedo-Mendoza, A.G.; Infantes-Molina, A.; Vargas-Hernández, D.; Chávez-Sánchez, C.A.; Rodríguez-Castellón, E.; Tánori-Córdova, J.C. Photodegradation of methylene blue and methyl orange with CuO supported on ZnO photocatalysts: The effect of copper loading and reaction temperature. *Mater. Sci. Semicond. Process.* **2020**, *119*, 105257. [[CrossRef](#)]
24. Van Huan, P.; Tam, P.D.; Pham, V.H. Visible-Light Photocatalysts of ZrO<sub>2</sub>/AgCl: Eu<sup>3+</sup> Nanoparticles. *J. Electron. Mater.* **2019**, *48*, 5294–5300. [[CrossRef](#)]
25. De Moraes, N.P.; de Azeredo, C.A.S.H.; Bacetto, L.A.; da Silva, M.L.C.P.; Rodrigues, L.A. The effect of C-doping on the properties and photocatalytic activity of ZrO<sub>2</sub> prepared via sol-gel route. *Optik* **2018**, *165*, 302–309. [[CrossRef](#)]
26. Zheng, J.; Sun, L.; Jiao, C.; Shao, Q.; Lin, J.; Pan, D.; Naik, N.; Guo, Z. Hydrothermally synthesized Ti/Zr bimetallic MOFs derived N self-doped TiO<sub>2</sub>/ZrO<sub>2</sub> composite catalysts with enhanced photocatalytic degradation of methylene blue. *Colloids Surf. A: Physicochem. Eng. Asp.* **2021**, *623*, 126629. [[CrossRef](#)]
27. Das, R.S.; Warkhade, S.K.; Kumar, A.; Wankhade, A.V. Graphene oxide-based zirconium oxide nanocomposite for enhanced visible light-driven photocatalytic activity. *Res. Chem. Intermed.* **2019**, *45*, 1689–1705. [[CrossRef](#)]
28. Majumder, D.; Chakraborty, I.; Mandal, K.; Roy, S. Facet-dependent photodegradation of methylene blue using pristine CeO<sub>2</sub> nanostructures. *ACS Omega* **2019**, *4*, 4243–4251. [[CrossRef](#)]
29. Zeleke, M.A.; Kuo, D.H. Synthesis and application of V<sub>2</sub>O<sub>5</sub>-CeO<sub>2</sub> nanocomposite catalyst for enhanced degradation of methylene blue under visible light illumination. *Chemosphere* **2019**, *235*, 935–944. [[CrossRef](#)]

- 
30. Quang, D.A.; Toan, T.T.T.; Tung, T.Q.; Hoa, T.T.; Mau, T.X.; Khieu, D.Q. Synthesis of CeO<sub>2</sub>/TiO<sub>2</sub> nanotubes and heterogeneous photocatalytic degradation of methylene blue. *J. Environ. Chem. Eng.* **2018**, *6*, 5999–6011.
  31. Yu, Z.; Chuang, S.S. Probing methylene blue photocatalytic degradation by adsorbed ethanol with in situ IR. *J. Phys. Chem. C* **2007**, *111*, 13813–13820. [[CrossRef](#)]